20 kHz 3-point bending fatigue of automotive steels

Mohamed Sadek[1,*], *Jens* Bergström[1], *Nils* Hallbäck[1] and *Christer* Burman[1]

[1]Karlstad University, Department of Engineering and Physics, SE-658 88 Karlstad, Sweden.

Abstract. The 20 kHz load frequency enables fatigue tests for very high cycle fatigue life, 10^9-10^{13} cycles, within conveniently short time. In automotive applications, many components are subjected to flexural loading and hence bending fatigue is an important test mode. Ultrasound fatigue test instruments have been used successfully in several assessments of fatigue strength and more commonly in uniaxial loading. Here, a 3-point bending fatigue test rig operating in resonance at 20 kHz load frequency has been designed to test plane specimens at R=0.1 loading. The test rig design and stress calculations are presented. Testing for fatigue strength was conducted using the staircase method with 15 specimens of each steel grade, specimens reaching 10^8 cycles were considered run-outs giving fatigue strength at 10^8 cycles. Additional 15 specimens of each grade were tested for S-N curves with the upper limit above 10^9 cycles. Two different common automotive steels, 38MnSiV5, a micro-alloyed ferritic-pearlitic steel, and 16MnCr5, a carburizing martensitic steel, were tested. The fatigue strengths achieved from the staircase testing are 340 and 419 MPa stress amplitudes for the 38MnSiV5 and 16MnCr5 steels, respectively. The S-N curves of the steels appear to be quite flat in the tested life range 10^7 – 10^9.

Keywords: Three-point bending, VHCF, automotive steels, ferritic-pearlitic steel, carburized steel

1 Introduction

Many components in automotive mechanical systems are subjected to cyclic flexural loading like bending or torsion. Hence the importance of investigating fatigue properties of automotive materials in these specific loading modes. During the last couple of decades, the development of the new fast fatigue testing system, the *Ultrasonic Fatigue Testing System*, have been taking place. The 20 kHz load frequency of the system enables fatigue tests for very high cycle fatigue life, 10^9-10^{13} cycles, within a conveniently short time, or significantly reduced test time and costs at shorter life. Ultrasound fatigue test instruments have been used successfully in several assessments of fatigue strength and more commonly in uniaxial loading. However, the development of special test rigs for other than uniaxial load modes in ultrasonic fatigue testing system, e.g. bending and torsion, has been taking place in various laboratories [1-4].

Components exposed to surface stress gradients are also often conveniently bestowed enhanced performance by surface strengthening using mechanical, thermal or thermochemical processes, and carburizing is one such method often used [5].

The aim using carburized steels is to obtain high-carbon plate type martensitic case with excellent wear and fatigue resistance and tough low-carbon core. Jo et al. [6] have studied the fatigue behaviour of carburized Cr-Mo gear steels subjected to multiaxial stress states. Axial and rotating bending have been performed at fully reversed loading (R=-1) and the results have been compared. The S-N curves they have achieved showed that the fatigue strength (at 10^6 cycles) in axial loading was ca 70% of the fatigue strength of rotating bending with surface initiation in the early lives ($<10^5$ cycles) and sub-surface initiations at longer lives ($>10^5$ cycles).

The fatigue strength of carburized steel depends on several factors, e.g. increased surface strength, residual stresses, modified microstructure, stress gradient, material hardness, surface roughness and surface oxidation.

Bomas et al. [7] have used Weibull´s weakest link concept to calculate a predicted fatigue limit for case-hardened 16MnCr5-steel grade. This model calculates

* Corresponding author: mohamed.sadek@kau.se

the 50% survival probability as the product of survival probability of the surface and the survival probability of the volume/core, Eq. 1.

$$P_s = P_s(A) * P_s(V) \quad (1)$$

Since the weakest link concept is based on the assumption that material strength is related to material imperfections, the calculated survival probability is depending not only on the load, rather also on the stressed volume.

In another study, Bomas et al. [8] have analysed the VHCF behaviour of 20MnCr5-steel grade with two different carburizing heat treatments yielding one superclean (nearly free of oxides) and one with normal content of non-metallic inclusions. The carburized layer depth (case-hardened depth, CHD) is 0,7 mm. The tests were conducted using an electro-magnetic resonant system (180-190 Hz) at two different loading ratios, R=-1 and R=0. Two different notched specimen geometries have been used, K_t=1,14 and K_t=1,21. Finite life and reduced fatigue strength was observed up to $2x10^8$ cycles. The initiation sites (regarding failure in VHCF regime) have been depending on several factors. Initiations were obtained exclusively in the interior at both non-defect sites and at non-metallic inclusions for the K_t=1,14. But for K_t=1,21, initiations in the carburized surface have also been observed. The weakest-link concept has again been used to predict the fatigue limit combined with the properties of the core and the carburized layer.

In the present work, a three-point bending fatigue test rig is designed and constructed to fit into the ultrasonic fatigue testing equipment to test plane specimens at R=0.1 loading. Two different automotive steels are investigated here; 38MnSiV5, a ferritic-pearlitic high strength micro-alloyed steel, and 16MnCr5, a carburizing martensitic steel grade. The complications with the three-point bend testing are most importantly holding the specimen in a fixed position to achieve the correct stress distribution in the specimen with maximal stress level at the specimen midsection.

2 Experimental

Two different steel grades are tested in the newly developed ultrasonic three-point bending fatigue testing system. The testing was aided by analytical and FEM computation of the deformation, strain and stress distribution in the specimen.

2.1. Materials

Two different common automotive steels were tested; 38MnSiV5 - a ferritic-pearlitic high strength micro-alloyed steel (Fig.1), in which normal contents of sulphide and oxide inclusions have been observed and 16MnCr5 - a carburizing martensitic steel grade (Fig.2) containing relatively high content of small sized sulphides and oxides to improve machinability. The carburizing, hardening and tempering cycle used was 900 ºC/3.5 h-860 ºC/2.5 h-oil quench 80 ºC-160 ºC/2 h, and this heat treat cycle exempt of carburizing was used on tensile test specimens to obtain the carburized core properties. The chemical composition of the two steel grades is presented in Table 1. Mechanical properties are presented in Table 2 (regarding the carburizing steel the given values are of the core).

Table 1. Chemical composition of the two steel grades.

Grade	C	Mn	Si	P	S	Cr
38MnSiV5	0,37	1,46	0,68	0,011	0,050	0,12
	Ni	**Mo**	**V**	**Cu**	**Al**	**Sn**
	0,10	0,03	0,10	0,12	0,014	0,009
	C	**Mn**	**Si**	**P**	**S**	**Cr**
16MnCr5	0,16	1,10	0,27	0,011	0,021	1,02
	Ni	**Mo**	**V**	**Cu**	**Al**	**Sn**
	0,11	0,03	0,01	0,14	0,021	0,009

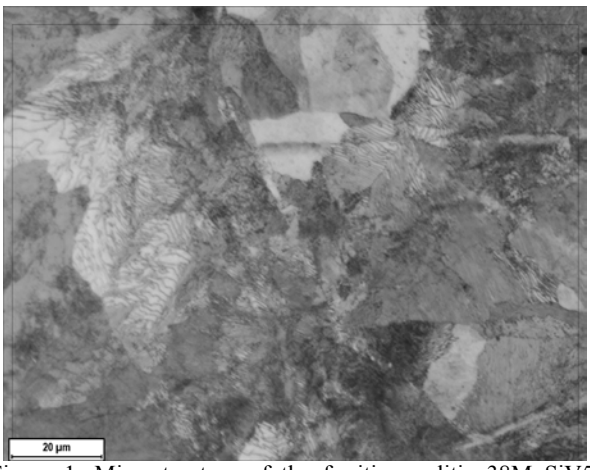

Figure 1. Microstructure of the ferritic-pearlitic 38MnSiV5-steel grade.

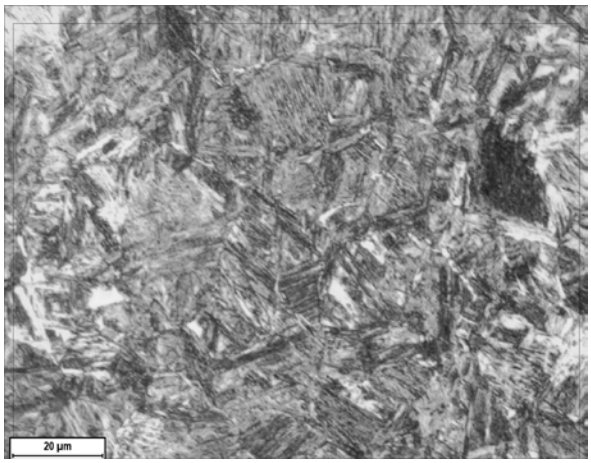

Figure 2. Microstrucure of the carburizing martensitic 6MnCr5-steel grade.

Table 2. Mechanical properties of the two steel grades. Core properties for the carburized 16MnCr5-steel grade.

Grade	Tensile Strength (MPa)	Yield Strength (MPa)	Hardness (HV30)
38MnSiV5	867	589	267
16MnCr5*	1175	876	438

As mentioned, the 16MnCr5-steel grade is a carburized martensitic steel. The carburizing treatment results in a higher carbon content at the surface elevating the surface hardness. The Vickers hardness profile is displayed in Fig. 3. The hardness profile indicates a carburized layer depth of ca 0.6 mm, corresponding to the depth of half of the hardness drop.

The surfaces of the specimen were ground and finally polished with 6 µm and then 3 µm polishing paste.

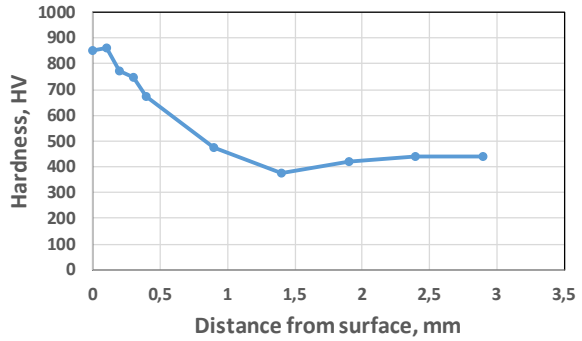

Figure 3. Vickers hardness profile for the carburized 16MnCr5-grade. Measured with a 25 gram load.

2.2. Instruments

A newly designed and build specimen holder is mounted on a self-aligning sliding bearing support (Fig. 4). The function of the holder is to keep the specimen in a fixed position regarding all directions.

The self-aligning support with the specimen holder are mounted into the ultrasonic fatigue testing system (Fig. 5). The low friction sliding bearing provides the alignment of the specimen holder in a plane perpendicular to the applied force direction.


Figure 4. Three-point bending specimen holder mounted on the Self-aligning supporter.

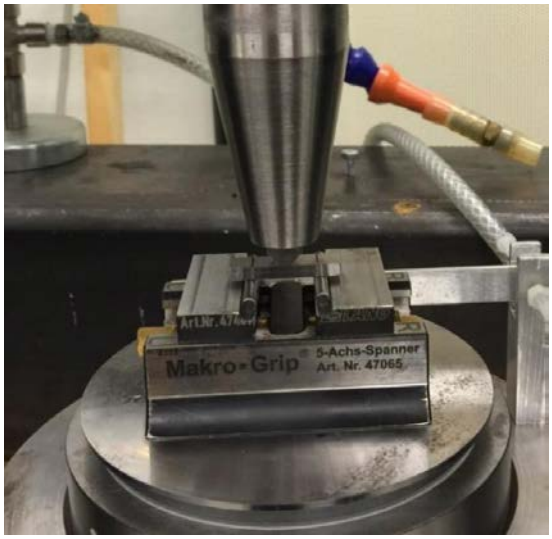

Figure 5. Specimen holder and Self-aligning supporter inserted into the ultrasonic fatigue testing system.

A specially designed metal tip is attached to the horn and transfers the load down to the specimen (Fig. 6). It is designed so that the load is transferred evenly across the

specimen width [3] and meets the resonance requirements of the system.

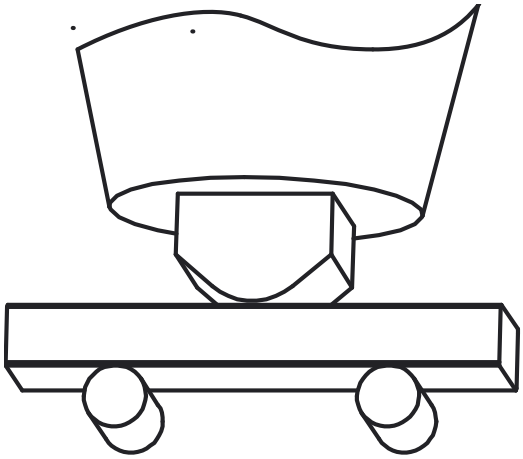

Figure 6. Load-transferring tip mounted into the horn.

For varying the load ratio *(R)* a mean static load is required. This static load is superimposed by mounting the whole load train together with the specimen holder and the self-aligning supporter into a mechanical screw test machine and loaded in compression. The two supporters have a diameter of 4 mm and are placed in tracks of approximately the same diameter allowing them to rotate freely.

Pressurized undercooled air is used to cool down the specimen and the surrounding parts during the testing.

2.2.1 Three-point bending specimen

The specimen used in this work is a rectangular bar specimen with 4x8 mm^2 cross-section and 31,8 mm length. To eliminate stress concentrations at the edges of the specimen, chamfers (0,2 mm deep at 45° angle) are milled at the edges.

2.3. Modelling and computation

The specific dimensions of the specimen are carefully chosen and tested with FEM for the steel specimen to have a flexural mode resonance frequency of 20 kHz. Analytical analysis of the specimen displacement (when under a cyclic load) has been derived elsewhere [4] and is presented in Eq. 2.

$$U(x) = A_0\left(\frac{\cosh(kL)}{\cos(kL)+\cosh(kL)}\right)* \left(\cos(kx)+\frac{\cos(kL)}{\cosh(kL)}\cosh(kx)\right) \quad (2)$$

where A_0 is the displacement at the middle of the specimen, L is the length of the specimen and k is the frequency dependent parameter given in Eq. 3.

$$k = \left(\frac{12\omega^2\rho}{Eh^2}\right)^{1/4} \quad (3)$$

where $\omega=2\pi f$ is the angular frequency, ρ is the material density, E is the elastic modulus and h is the height of the specimen. From the same analytical procedure, the specimen's resonance length *(L)* and the required distance between the supporters *(L_0)* are defined as in Eq. 4-5.

$$2L = 0{,}506925\left(\frac{Eh^2}{\rho f^2}\right)^{1/4} \quad (4)$$

$$2L_0 = 0{,}27966\left(\frac{Eh^2}{\rho f^2}\right)^{1/4} \quad (5)$$

These expressions were used as guidelines to select the proper test and specimen geometries in the present study. Final calculations of the test set-up were done using FEM and the Abaqus software. As well, FEM was used to compute the stress amplitudes and distribution in the specimen (Fig. 7). For varying loading ratio, both static and dynamic stress components are required, i.e. a mean load *(σ_m)* and a sinusoidal stress amplitude *(σ_a)*, Eq. 6.

$$\sigma(t) = \sigma_m + \sigma_a \sin(\omega t) \quad (6)$$

Both the static mean load and the dynamic stress amplitude are related to the maximum displacement of the specimen (at the mid-section of the specimen directly under the load-transferring tip), calculated by static and dynamic FEM simulations respectively. Fig. 8 shows the stress distribution and the maximum stresses for a displacement of 20 µm. For the cyclic stress amplitude *(σ_a)* the so-called m-factor is needed to control testing. The m-factor correlates the maximum stress amplitude to the displacement, Eq. 7, since the control parameter during testing is the displacement at the bottom of the horn (this displacement is calibrated against the ultrasound generator voltage input to the oscillator directly controlled by the operator).

$$m_{amp} = \frac{\sigma_{a,max}}{U} = \frac{226\ MPa}{20\ \mu m} = 11{,}3\ MPa/\mu m \quad (7)$$

The mean stress *(σ_m)* is controlled by the force input in the tensile testing machine. Hence the m-factor for the mean load is a correlation between the statically determined maximum stress and the force acting on the specimen, Eq. 8.

$$m_{mean} = \frac{\sigma_{m,max}}{F} = \frac{220{,}5\ MPa}{1104\ N} = 0{,}1997\ MPa/N \quad (8)$$

Here, a load ratio of *R=0,1* was used in all cases.

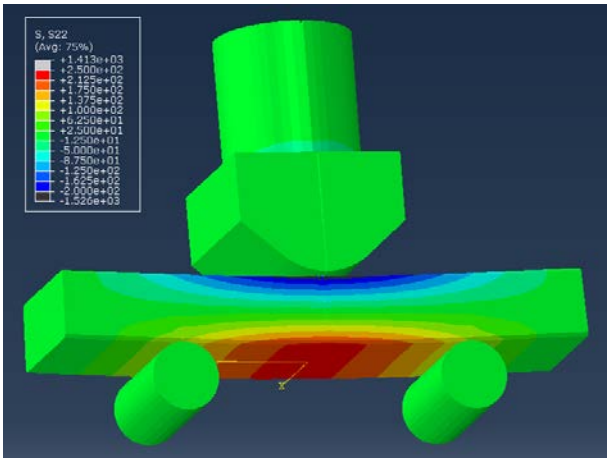

Figure 7. Stress distribution in the specimen shown with a FEM model.

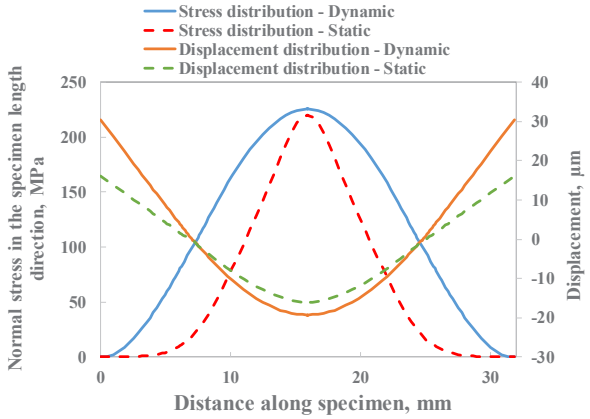

Figure 8. Stress and displacement distribution along specimen's length in dynamic and static simulations.

2.4. Testing

Testing for fatigue strength was conducted using the staircase method with 15 specimens of each steel grade. The tests were stopped at 10^8 cycles and the specimens surviving were considered run-outs, which defines the obtained fatigue strength at 10^8 cycles [9]. If a specimen fails prior to the run-out life, the next specimen is tested at a lower stress level, but if the specimen survives until run-out the next specimen is tested at a higher stress level. The increments are usually around 5% of the mean fatigue limit. For the data reduction technique, here the Dixon-Mood [10] technique was used, yielding both the fatigue strength and the standard deviation.

Additional 15 specimens of each steel grade were tested for the S-N curves with the upper limit above 10^9 cycles. The evaluation of the S-N curves was done according to the SS-ISO12107 standard [11] Linear Fatigue Response, as in Eq. 9,

$$Log_{10}(N) = b_0 + b_1\, Log_{10}(S) \qquad (9)$$

from where also the regression parameters b_0 and b_1 were estimated.

3 Results

The new constructed rig for three-point bending fatigue testing at 20 kHz worked appropriately. The specimen was held in a fixed position and the loading was performed correctly.

The fatigue strength (σ_{FL}) at 10^8 cycles and the standard deviation yielded by the staircase testing are presented in Table 3.

Table 1. Fatigue strength at 10^8 load cycles and standard deviation for the two steel grades.

Steel grade	σ_{FL}	Standard deviation
38MnSiV5	340 MPa	±10 MPa
16MnCr5	419 MPa	±14 MPa

The S-N curves of the two materials are displayed in Fig. 9. The evaluation according to the SS-ISO12107 standard were performed on the results of both materials. The red line in Fig. 9 represent the predicted fatigue strength for the 38MnSiV5-steel grade according to Eq. 9 with life as depending variable. For the 16MnCr5-steel grade the predicted fatigue strength showed a significant deviation from the results, hence it is not plotted here. Instead, a regression line using life as independent variable is inserted. The regression parameters according to the standard are presented in Table 4.

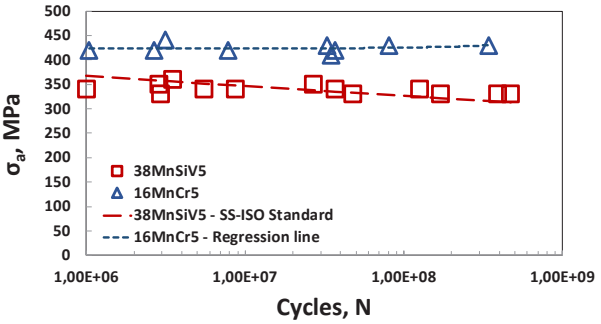

Figure 9. S-N curves of the two steel grades and the predicted S-N curve for the 38MnSiV5-grade according to Eq. 9.

Table 2. Regression parameters according to the SS-ISO12107 standard.

Grade	b_0	b_1	R^2
38MnSiV5	105,08	-38,63	0,28
16MnCr5	-16,41	8,99	0,01

As observed in Fig. 9, the S-N curves of both steel grades has a flat appearance in the 10^6 – 10^9 range, thus

the fatigue life range is quite large at that level of fatigue strength.
A study of the fracture surfaces was performed using a high resolution FEG-SEM LEO scanning electron microscope. The initiation sites were found to be at the flat surface, in the corners and even in the interior (close to the surface) for the 38MnSiV5-steel grade, but exclusively in the corners for the 16MnCr5-steel grade. Figures 10-12 shows some examples of typical fracture surfaces.

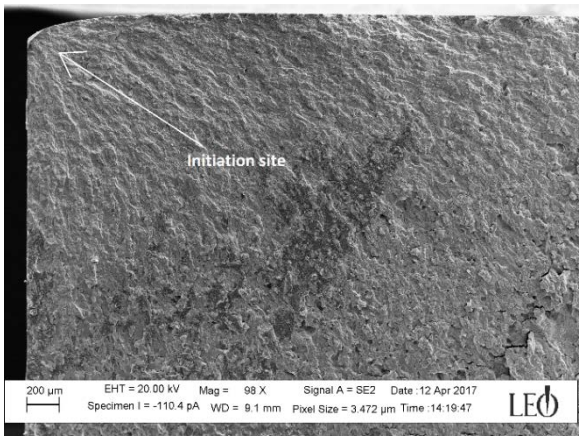

Figure 10. Crack initiation at the corner, 38MnSiV5-steel grade. σ_a=340 MPa and N_f=10^6 cycles.

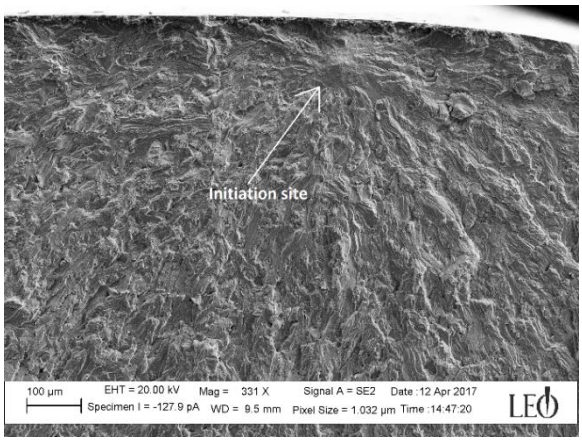

Figure 11. Interior crack initiation close to the surface with a FGA formation, 38MnSiV5-steel grade. σ_a=330 MPa and N_f=3,9*10^8 cycles.

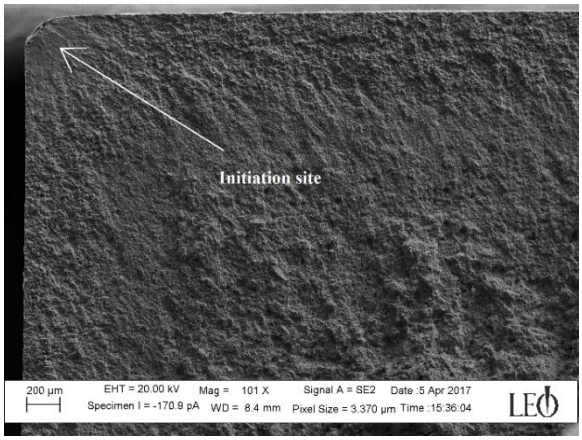

Figure 12. Crack initiation at the corner, 16MnCr5-steel grade. σ_a=420 MPa and N_f=7,8*10^6 cycles.

4 Discussion

During the development of the new three-point bending rig, several complications were encountered. One problem was the alignment of the specimen perpendicular to the load direction. This was elegantly solved by mounting the specimen holder onto a self-aligning support at the bottom of the load train (Fig. 4-5) with the eucentric rotation at the point of load tip contacting the specimen surface. With this solution, the specimen is aligned during the application of the mean load and keeps the position during the rest of the test. Furthermore, the friction between the specimen and the supports and the surrounding position constraining parts caused wear and elevated temperatures. This problem was handled by delicate positioning of the surrounding constraining parts.

The precision of the sinusoidal loading *(σ_a)* is depending on the step size of the voltage input, which is 0,1 V in the current ultrasonic fatigue testing system. With the calculated m-factor (Eq. 7) and the displacement calibration, the precision of stress amplitude *(σ_a)* for the used setup with the specific horn dimensions is calculated to ±5 MPa (corresponding to 0,5 µm displacement). The maximum possible stress amplitude *(σ_a)* with the current setup is ca 950 MPa (corresponding to 84 µm displacement) due to the maximum voltage input of ca 9 V. The precision percentage is hence 0,5/84=0,6%.

Evidently, the S-N curves of the steels appears to be quite flat in the tested life range 10^6 – 10^9. These shapes have been seen in the results from 20 kHz uniaxial fatigue testing of the same materials at the same loading ratio *(R=0,1)* [12]. It is speculated whether fatigue crack initiation mechanisms controlling life are different at short and long lives. Further comparison to the uniaxial loading results, shows that the S-N curve of the 38MnSiV5-steel grade is quite higher (ca 60 MPa) for the three-point bending tests. For the 16MnCr5-steel grade however, the S-N curves of three-point bending and uniaxial testing showed good agreement. Commonly, one expects higher fatigue strength in bending than in tension fatigue, as [6] have found where the results showed that the fatigue strength of the uniaxial loading tests were about 70% of the fatigue strength of the rotating bending testing. However, surface conditions may play an important role. Thus, the less defect sensitive 38MnSiV5 will gain in bending, while the opposite holds for the carburized 16MnCr5 steel. As a consequence, the 16MnCr5 fatigue strength in tension is 1.6 times larger than that that of the 38MnSiV5 steel, but in bending only 1.2 times larger.

The fractography study showed that the initiation sites for the 38MnSiV5-steel grade were distributed between the bottom surface, bottom corners and even some interior initiations close to the surface. While for the 16MnCr5-steel grade, the carburized layer elevates the material strength and possibly creates some residual stresses at the surface. The effect of this was restriction

of the initiation sites to the bottom corners of the specimen. The fact that, for carburized specimens, the initiation sites are rather found in the interior is confirmed by [8, 12] where surface initiations were observed only on specimens with a relatively high stress concentration factor, K_t.

5 Conclusion

The development and exploration of a new bending fatigue test rig operating at 20 kHz load frequency has been presented. Careful design of operation proved the test rig to run efficiently and to produce reliable results. Finite fatigue lives between 10^6 and 10^9 load cycles were obtained of the ferritic-pearlitic and carburized martensitic steels, and similar to tests in tension fatigue flat SN-curves were obtained. The mechanisms responsible of this behaviour are still left to be determined. The increase in fatigue strength using the carburized grade rather than the ferritic-pearlitic steel was much smaller in bending than in tension fatigue, contrary to what expected.

6 Acknowledgements

The research leading to these results has received funding from the EuropeanUnion's Research Fund for Coal and Steel (RFCS) research programme under grant agreement no. [RFS-CT-2013-00015 (FREQTIGUE)].

References

1. W. Hoffelner, Journal of Physics, E: Scientific Instruments, **13(6):** p. 617 (1980)
2. W. Hoffelner, P. Gudmundson, Engineering fracture mechanics, **16(3)**: p. 365-371 (1982)
3. H.Q. Xue, et al., International Journal of Fatigue, **29(9-11):** p. 2085-2093 (2007)
4. C. Bathias, P.C. Paris, *Giga cycle fatigue in mechanical practice*, Marcel Dekker (2005)
5. Bergström, J., et al, Final report RFS-CT-2013-00015 (FREQTIGUE). 2018.
6. B. Jo, S. Sharifimehr, Y. Shim, A. Fatemi, International Journal of Fatigue, **100**: p. 454-465 (2017)
7. H. Bomas, P. Mayr, M. Schleicher, Materials Science and Engineering **A234-236:** p. 393-396 (1997)
8. H. Bomas, K. Burkart, H.W. Zoch, International Journal of Fatigue **60:** p.63-73 (2014)
9. Y.-L. Lee, *Fatigue testing and analysis: theory and practice*, Elsevier (2005)
10. W.J. Dixon, A.M. Mood, Journal of the American Statistical Association, **43(241):** p. 109-126 (1948)
11. *SS-ISO 12107, Metallic materials – Fatigue testing – Statistical planning and analysis of data* (2012)
12. M. Sadek, J. Bergström, N. Hallbäck, C. Burman, R. Elvira, B. Escauriaza, *Seventh International conference on Very High Cycle Fatigue (VHCF7) Proceedings*, **7:** p. 193-198 (2017)